Dalton Transactions

Accepted Manuscript

ROYAL SOCIETY OF CHEMISTRY

www.rsc.org/dalton

Dalton Transactions Dalton Transactions Dynamic Article Links ▶

Cite this: DOI: 10.1039/c0xx00000x

www.rsc.org/xxxxxx

PAPER

A Family of Enantiopure Fe^{III}_4 Single Molecule Magnets: Fine Tune of Energy Barrier by Remote Substituent†

Yuan-Yuan Zhu,[a,b] Chang Cui,[b] Kang Qian,[b] Ji Yin,[a] Bing-Wu Wang,*[b] Zhe-Ming Wang,[b] and Song Gao*[b]

Received (in XXX, XXX) Xth XXXXXXXXX 20XX, Accepted Xth XXXXXXXXX 20XX
DOI: 10.1039/b000000x

A new family of enantiopure star-shaped Fe^{III}_4 single-molecule magnets (SMMs) with the general formula $[Fe_4(L^K)_6]$ (H_2L = (*R* or *S*)-2-((2-hydroxy-1-phenylethylimino methyl)phenol)), K = H (**1**), Cl (**2**), Br (**3**), I (**4**), and *t*-Bu (**5**)), were structurally and magnetically characterized. The complex **1** has been reported in our previous paper (*Chem. Commun*. **2011**, *47*, 8049–8051). Detailed magnetic measurements and systematic magneto-structural correlation study revealed that the SMM properties of this series of compounds can be finely tuned by the remote substituent of the ligands. Although the change in the coordination environment of the central Fe^{3+} ions is very small, the properties of SMM behavior are changed considerably. All five complexes display frequency dependence of the ac susceptibility. However, the χ_{ac}'' peaks of complexes **2** and **5** cannot be observed down to 0.5 K. The fitted anisotropy energy barriers (U_{eff}) of complexes **1**, **3**, and **4** were 5.9, 7.1, and 11.0 K, respectively. Moreover, the hysteresis loops of these three complexes can be also observed around 0.5 K. Magneto-structural correlation analyses revealed that the coordination symmetry of central Fe^{3+} ion and the intermolecular interaction are two key factors to affect the SMM properties. The deviation to trigonal prism coordination environment and the existence of intermolecular interaction between the neighboring clusters may both reduce the anisotropy energy barriers.

Introduction

Since the first Single-molecule magnets (SMMs) $Mn_{12}OAc$, that an individual molecule showed superparamagnetic behavior below a certain blocking temperature, was discovered in 1990s,[1] a lot of deep researches and continuous development have focused on exploring this new scientific field owing to their unique magnetic properties and potential applications in information storage and quantum computing.[2, 3] Many synthetic efforts were made to obtain new SMMs with a higher blocking temperature by the modulation of ground-spin states (*S*) and axial zero-field splitting parameter (*D*). Usually, the big *S* can be obtained by increasing the paramagnetic centers coupled by ferromagnetic or antiferromagnetic interactions in the cluster. However, the enhancement and control of *D* are relatively difficult. In a cluster-type molecule, the *D* value is dependent on the local anisotropy of the single ions and their vectorial addition, the unparallel arrangement of axial anisotropy of spin carriers may reduce even vanish the zero-field splitting (ZFS). Up to now, several SMMs families, such as Mn_{12},[1,4] Mn_6,[5] and Fe_4[6] molecules were reported. In pursuit of understanding the origin and impact factor of magnetic anisotropy of these SMMs, consecutive effort has been paid to synthesize structure-tuned molecules with the same skeleton. Some groups proposed and applied site-specific modification strategy to obtain a family molecules aim to understand the magneto-structural correlation and enhance the energy barrier. This strategy was first applied in the chemistry of famous Mn_{12} family. The systematic research works by Gatteschi, Sessoli, Hendrickson, Christou, and co-workers have constructed many Mn_{12} derivatives with controlled ligand replacement, which demonstrated small perturbations on the magnetic anisotropy can change the relaxation barriers.[1,4] Another successful example applying site-specific modification strategy is Fe_4 family SMMs.[6] Fe_4 SMMs belong to the tetranuclear star-shaped clusters, which are comprised of a central ion and three peripheral ions. This series of molecules is a relatively simple system that shows SMMs behavior. Several clusters with similar skeleton such as Cr^{III}_4,[7] Mn^{II}_4,[8] Ni^{II}_4,[9] $Cr^{III}Mn^{II}_3$,[10] $Cr^{III}Fe^{III}_3$,[11] and $Co^{II}Co^{III}_3$[12] with intriguing magnetic properties have been reported. After the archetype Fe_4 SMM was reported in 1999, several new Fe_4 SMMs were obtained by replacing the axial ligand or using new ligands.[6,13] Systematic magneto-structure correlation revealed the energy barrier can be enhanced when the symmetry of the Fe_4 molecules was raised from C_2 to D_3. In recent years, some important progresses in spintronics make Fe_4 clusters being one of the most important SMMs again. Because of their ease in the modification of axial ligands and their stability in vacuum, Fe^{III}_4 clusters can stick on silicon,[14] gold surface,[15] or carbon nanotubes[16] through immobilization and provide fascinating examples for the single-molecule magnetic behavior on surface or magnetic property

studies on monolayer molecule assemble. With the aid of X-ray magnetic circular dichroism (XMCD) technique, Sessoli and Cornia et al characterized the magnetic properties of a Fe^{III}_4 SMM on the gold surface and confirmed that the Fe^{III}_4 molecule reserved the SMM behavior on the surface.[15] It is an exciting result for the potential applications of SMMs in molecular spintronics, ultrahigh-density information storage, or quantum computing.

Recently, the development of enantiopure chiral molecule-based magnets has been a topic of growing interest for synthetic chemists.[17,18] Chiral Magnet has opened up a new field of research on molecular materials possessing both magnetic and optical properties. Such materials appear to be good candidates to present a cross effect between circular dichroism (CD) and magneto-chiral dichroism (MChD).[19] Some reports demonstrated enantiopure magnets can be obtained by spontaneous resolution method during crystal growth in the absence of a chiral source.[20] However, from a synthetic point of view, such process was not suitable to be considered as a preparative method because it is difficult to control the absolute configuration and obtain enantiopure chiral crystals. A practical approach to obtain enantiopure molecular magnets is to synthesize the chiral ligands enantioselectively, and then transfer the chiral information to the paramagnetic assemblies through coordination bonds. Up to now, most reported chiral magnets were multidimensional magnetic ordering materials, the examples of chiral SMM were rare.[12,13,20d]

Though the sum of reported Fe_4 SMMs in literature has already exceeded twenty,[6] the chiral example is still rare.[6j,13] The chiral Fe_4 SMMs will not only expand the Fe_4 family but also afford new interesting example of multifunctional SMMs, and provide possible candidate for molecular spintronics devices. Very recently, our group has found that several chiral Fe^{III}_4 type SMMs can show optical activity simultaneously. In 2011, we reported a pair of novel chiral star-shaped Fe^{III}_4 compounds showed SMM behavior.[13] As a continuation of preliminary work, we tune finely the coordination environment of central Fe^{3+} ion by remote substituting the ligand to understand the magneto-structure correlation of this series of Fe^{III}_4 SMMs and improve the anisotropy energy. The Schiff base ligand used in our previous work can be easily modified by introducing substitutes in the *p*-position of salicylaldehyde ring, which facilitates us to obtain a series of Fe^{III}_4 clusters with the same star shaped skeleton. In this article, we report the preparation, magnetism, magneto-structural correlation analysis, and chirality of five new star-shaped Fe^{III}_4 compounds with different substituent Schiff base ligands.

Experimental Section

Reagents and General Procedures

All starting materials were commercially available at analytical grade and used without further purification. All reactions were carried out under aerobic condition.

Synthesis of ($[Fe_4(L^{Cl}_R)_6]\cdot 4DMF$) (2*R*) and ($[Fe_4(L^{Cl}_S)_6]\cdot 4DMF$) (2*S*)

A mixture of $H_2L^{Cl}_R$ (414 mg, 1.5 mmol) and Et_3N (4.3 mL, 3 mmol) in methanol (20 mL) was stirred at room temperature. A brown precipitate was generated as soon as the solution of $FeCl_2$ (198 mg, 1 mmol) in methanol (10 mL) was added dropwise (the Fe ions were oxidated from +2 valence to +3 valence in the air immediately). Then the mixture was stirred further at room temperature for 12 h. The resulting solution was filtered and the solvent was removed under vacuum. The brown precipitate was dried under vacuum then redissolved in hot DMF (40 mL). Dark brown chunks were obtained within two weeks in 70–80% yield by slow evaporation of the resulting solution. The crystals are stable at room temperature and no loss of solvent is observed. Anal. Calcd for $C_{102}H_{100}Cl_6Fe_4N_{10}O_{16}$: C, 56.77; H, 4.67; N, 6.49. Found: C, 56.73; H, 4.68; N, 6.54. IR (pure sample): ν = 3651(w), 3060(w), 3029(w), 2915(w), 2860(w), 2700(w), 2635(w), 1956(w), 1888(w), 1817(w), 1751(w), 1674(m), 1628(s), 1530(m), 1459(s), 1417(w), 1377(w), 1362(m), 1328(w), 1309(m), 1264(w), 1246(w), 1175(m), 1132(w), 1088(m), 1068(m), 1042(m), 1030(m), 1002(w), 984(w), 943(w), 918(w), 874(w), 826(m), 809(m), 762(w), 733(w), 702(m), 660(m), 640(w). HRMS (ESI): Calcd. For $C_{90}H_{73}Cl_6Fe_4N_6O_{12}^+$: 1863.0811. Found: 1863.0832.

The enantiomer complexes of **2*S*** ($[Fe_4(L^{Cl}_S)_6]\cdot 4DMF$) was synthesized by using $H_2L^{Cl}_S$ as ligand in the same way. Yield: 70%. Anal. Calcd for $C_{102}H_{100}Cl_6Fe_4N_{10}O_{16}$: C, 56.77; H, 4.67; N, 6.49. Found: C, 56.70; H, 4.67; N, 6.53. IR (pure sample): ν = 3651(w), 3061(w), 3029(w), 2915(w), 2861(w), 2701(w), 2635(w), 1955(w), 1889(w), 1752(w), 1675(m), 1629(s), 1530(m), 1493(w), 1460(s), 1417(m), 1377(m), 1363(m), 1310(m), 1265(w), 1244(w), 1196(w), 1175(m), 1132(w), 1088(w), 1068(m), 1042(m), 1030(m), 1002(w), 983(w), 943(w), 919(w), 874(w), 826(m), 809(m), 762(w), 733(w), 702(m), 661(m), 641(w).

Synthesis of ($[Fe_4(L^{Br}_R)_6]\cdot 5.5DMF\cdot 0.5MeOH$) (3*R*)

Compound **3*R*** was synthesized by using $H_2L^{Br}_R$ as the ligand in the same way. Yield: 75%. Anal. Calcd for $C_{107}H_{112.5}Br_6Fe_4N_{11.5}O_{18}$: C, 50.39; H, 4.45; N, 6.32. Found: C, 50.05; H, 4.60; N, 6.50. IR (pure sample): ν = 3650(w), 3052(w), 3029(w), 2917(w), 2861(w), 2698(w), 2634(w), 1956(w), 1890(w), 1817(w), 1748(w), 1675(m), 1626(s), 1591(w), 1527(m), 1493(w), 1461(s), 1414(w), 1376(m), 1328(m), 1307(w), 1256(w), 1195(w), 1175(m), 1134(w), 1089(w), 1068(m), 1042(m), 1002(w), 986(w), 942(w), 913(w), 875(w), 825(m), 807(m), 763(w), 704(m), 690(m), 649(m). HRMS (ESI): Calcd. For $C_{90}H_{73}Br_6Fe_4N_6O_{12}^+$: 2132.7754. Found: 2132.7749.

Synthesis of ($[Fe_4(L^{I}_R)_6]\cdot 5.5DMF\cdot 0.5MeOH$) (4*R*)

Compound **4*R*** was synthesized by using $H_2L^{I}_R$ as the ligand in the same way. Yield: 70%. Anal. Calcd for $C_{108}H_{114}I_6Fe_4N_{12}O_{18}$: C, 45.47; H, 4.03; N, 5.89. Found: C, 45.80; H, 3.95; N, 5.65. IR (pure sample): ν = 3663(w), 3052(w), 3030(w), 2918(w), 2862(w), 2699(w), 2634(w), 2270(w), 1957(w), 1891(w), 1818(w), 1675(s), 1625(s), 1591(w), 1527(m), 1493(m), 1461(s), 1413(m), 1376(m), 1362(m), 1328(m), 1306(s), 1256(w), 1195(w), 1175(m), 1134(w), 1090(m), 1068(m), 1042(m), 1002(w), 989(w), 941(w), 912(w), 875(w), 825(m), 806(m), 763(m), 705(m), 689(m), 649(m).

Synthesis of ($[Fe_4(L^{t\text{-}Bu}_R)_6]\cdot 6DMA$) (5*R*)

Compound **5*R*** was synthesized by using $H_2L^{t\text{-}Bu}_R$ as the ligand in the same way, and was recrystallized in DMA. Yield: 65%. Anal. Calcd for $C_{138}H_{180}Fe_4N_{12}O_{18}$: C, 65.82; H, 7.20; N, 6.67. Found:

C, 66.02; H, 7.22; N, 6.87. IR (pure sample): ν = 3060(w), 3027(w), 2958(m), 2904(m), 2864(m), 2710(w), 1954(w), 1889(w), 1815(w), 1760(w), 1682(m), 1624(s), 1534(m), 1474(m), 1455(m), 1416(w), 1381(m), 1362(m), 1315(m), 1267(m), 1254(m), 1212(w), 1177(m), 1145(w), 1110(w), 1069(m), 1045(m), 1030(m), 1002(w), 985(w), 947(w), 882(w), 843(m), 831(m), 810(w), 761(w), 749(w), 702(m), 669(w), 642(w), 614(w). HRMS (ESI): Calcd. For $C_{114}H_{127}Fe_4N_6O_{12}^+$: 1996.69433. Found: 1996.69805.

Table 1 Crystal data, data collection, solution, and refinement information of compounds **2**–**5**

	2 (*R*)	**2** (*S*)	**3** (*R*)	**4** (*R*)	**5** (*R*)
Formula	$C_{102}H_{100}Cl_6Fe_4N_{10}O_{16}$	$C_{102}H_{100}Cl_6Fe_4N_{10}O_{16}$	$C_{107}H_{112.5}Br_6Fe_4N_{11.5}O_{18}$	$C_{108}H_{114}Fe_4I_6N_{12}O_{18}$	$C_{138}H_{180}Fe_4N_{12}O_{18}$
Formula weight	2158.02	2158.02	2550.45	2852.91	2518.34
Crystal system	orthorhombic	Orthorhombic	monoclinic	monoclinic	monoclinic
Space group	$P2_12_12_1$	$P2_12_12_1$	$P2_1$	$P2_1$	$P2_1$
a, Å	20.880(6)	20.925(4)	12.475(2)	12.484(3)	17.7804(3)
b, Å	21.762(6)	21.788(4)	19.361(4)	19.542(4)	21.4247(4)
c, Å	22.215(5)	22.222(4)	24.438(5)	24.631(5)	18.2283(4)
α, deg	90	90	90	90	90
β, deg	90	90	104.566(2)	104.65(3)	91.988(2)
γ, deg	90	90	90	90	90
V, Å^3	10094(5)	10132(3)	5713.1(18)	5814(2)	6939.7(2)
Z	4	4	2	2	2
T, K	173(2)	173(2)	173(2)	173(2)	180(2)
F(000)	4464	4464	2586	2824	2680
D_C, g cm^{-3}	1.420	1.415	1.483	1.630	1.205
μ, mm^{-1}	0.792	0.789	2.663	2.149	0.475
λ, Å	0.71073	0.71073	0.71073	0.71073	0.71073
Crystal size, mm^3	0.44 × 0.36 × 0.20	0.72 × 0.70 × 0.65	0.36 × 0.26 × 0.17	0.36 × 0.32 × 0.31	0.35 × 0.25 × 0.15
T_{min} and T_{max}	0.7453, 0.8484	0.7291, 1.0000	0.3422, 0.5950	0.6950, 1.0000	0.74923, 1.0000
θ_{min}, θ_{max}, deg	1.3099, 25.3366	0.9731, 26.0179	1.3592, 27.4691	1.0420, 27.4844	3.2670, 27.1320
no. total reflns.	65865	58679	46812	39344	48179
no. uniq. reflns, R_{int}	18428, 0.0668	19848, 0.0796	24523, 0.0702	23874, 0.0423	25359, 0.0265
no. obs. [$I \geq 2\sigma(I)$]	17653	18332	19710	22673	21372
no. params	1251	1251	1310	1333	1587
$R1$ [$I \geq 2\sigma(I)$]	0.0599	0.0770	0.0981	0.0687	0.0604
$wR2$ (all data)	0.1659	0.2019	0.1949	0.2071	0.1719
S	1.245	1.238	1.137	1.110	1.039
$\Delta\rho^a$, e/ Å^3	0.644, –0.969	0.661, –0.925	0.837, –0.742	1.739, –1.236	1.150, –0.447
max and mean Δ/σ^b	0.001, 0.000	0.000, 0.000	0.000, 0.000	0.001, 0.000	0.001, 0.000
Flack parameter	0.054(15)	0.043(18)	0.062(11)	0.05(2)	–0.022(13)

Single-crystal X-ray diffraction

Single-crystal X-ray diffraction measurements of **2*R***, **2*S***, and **3*R*** were carried on a Saturn724+ CCD diffractometer with graphite-monochromator Mo-Kα radiation (λ = 0.71073 Å) at 173 K. Intensities were collected using CrystalClear (Rigaku Inc., 2008) technique and absorption effects were collected using the Numerical technique. Single-crystal X-ray diffraction measurements of **1*S*** and **4*R*** were carried on a Saturn724+ CCD diffractometer with Confocal-monochromator Mo-Kα radiation (λ = 0.71073 Å) at 173 K. Intensities were collected using CrystalClear (Rigaku Inc., 2008) technique and absorption effects were collected using the multi-scan technique. Single-crystal X-ray diffraction measurement of **5*R*** was collected on an Agilent Technologies SuperNova Atlas Dual system with a (Mo) microfocus source and focusing multilayer mirror optics.

The structure of all compounds was solved using SHELXS-97 program[21] and refined by a full matrix least squares technique based on F^2 using SHELXL 97 program.[22]

Magnetic measurement and other physical Techniques

Magnetic measurements were performed on a Quantum Design MPMS XL-5 SQUID magnetometer on polycrystalline samples. Data were corrected for the diamagnetism of the samples using Pascal constants and of the sample holder by measurement. The experiments below 1.8 K were measured on the *i*Helium Measurement Console in coordination with MPMS XL-5 SQUID magnetometer.

The axis and transverse zero-field splitting parameters D and E were calculated with the DFT method at the B3LYP/TZVP level of theory for the central Fe^{3+} ion and six coordinated oxygen atom of this series compounds. Hydrogen atoms were added theoretically to balance the charge. All the computations were performed in the ORCA package. The computational details are provided in ESI.

CD spectral measurements in solution and solid state were performed on a JASCO J-815 CD spectropolarimeter.

Results and Discussion

Synthesis of the Fe^{III}_4 complexes.

In this work, besides H_2L, four new Schiff base type ligands with different substituent in the *p*-position of salicylaldehyde ring were used to construct the Fe^{III}_4 clusters. The structures of the five ligands are listed in Chart 1. This series Schiff base ligands can be synthesized by the condensation of (*R* or *S*)-2-amino-2-phenylethanol with corresponding salicylaldehyde derivatives in ethanol. The pure needlelike crystalline products were obtained by recrystallization in the mixed solvent of ethyl acetate and petroleum ether with high yield.

Series of complexes **1–5** were obtained by the reaction of $FeCl_2{\cdot}4H_2O$, H_2L, and Et_3N in methanol (see experimental

section). The pure products were recrystallized as block crystals in DMF or DMA solution. The color of **1**(*R* and *S*), **2**(*R* and *S*), **3**(*R*), **4**(*R*), and **5**(*R*) are dark brown. The structures of six complexes **1*R***–**5*R*** were characterized by single crystal X-ray analysis, and also the enantiomer structures of **1*S*** and **2*S***.

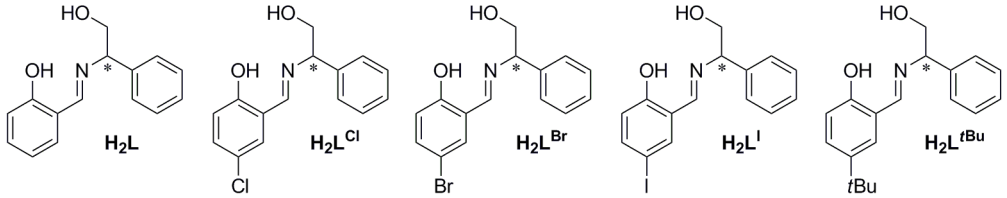

Chart 1 The structure of Schiff base ligands with different substituent in the *para* position.

Solid-state Structure

Although the five complexes have similar star-shaped Fe^{III}_4 skeleton, they crystallized in different space group. Compound **1**, **3**, **4**, and **5** belong to $P2_1$ space group and compound **2** belong to $P2_12_12_1$ space group, respectively. In all Fe^{III}_4 complexes, four Fe^{3+} ions (one central Fe^{3+} ion and three peripheral Fe^{3+} ions) are located in the same plane.

The structural details of Compounds **1*R*** and **1*S*** have been descripting in our previous report.[13] These clusters both possess pseudo C_3 molecule symmetry.

Compounds **2*R*** and **2*S*** crystallize in the orthorhombic space group $P2_12_12_1$. The unit cell comprises four clusters and sixteen DMF molecules. The distances between the central Fe^{3+} ion and three peripheral Fe^{3+} ions are slightly different. For **2*R*** as example, the Fe···Fe distances are 3.232(1) Å for Fe1–Fe2, 3.234(1) Å for Fe1–Fe3, and 3.240(1) Å for Fe1–Fe4. Three edges of the iron triangle are not exactly the same, with 5.466(1) Å for Fe2–Fe3, 5.553(1) Å for Fe3–Fe4, and 5.778(1) Å for Fe4–Fe2. The coordination environment of the central Fe1 ion is composed of six oxygen atoms with Fe1···O distances ranging from 2.005(4) Å to 2.048(4) Å. It is in *pseudo* C_3 symmetry and forms a slightly distorted triangular prism, which is similar to that in **1**. The selected bond distances and angles for **2*R*** and **2*S*** are listed in Table S1 and S2.

Compound **3*R*** crystallizes in the monoclinic space group $P2_1$, the same space group as the archetype compound **1**. The unit cell comprises two clusters, eleven DMF molecules, and one methanol molecule. Similar to **2**, the distances between the central Fe^{3+} ion and three peripheral Fe^{3+} ions are also slightly different. The Fe···Fe distances are 3.218(2) Å for Fe1–Fe2, 3.223(2) Å for Fe1–Fe3, and 3.236(2) Å for Fe1–Fe4. Three edges of the iron triangle are not exactly the same, with 5.543(2) Å for Fe2–Fe3, 5.634(2) Å for Fe3–Fe4, and 5.580(2) Å for Fe4–Fe2. The coordination environment of the central Fe1 ion in **3*R*** has *pseudo* C_3 symmetry with Fe1···O distances ranging from 2.007(6) Å to 2.049(6) Å, and forms a slightly distorted triangular prism. The selected bond distances and angles for **3*R*** are listed in Table S3.

The structure of Compound **4*R*** is similar with **3*R***. It also crystallizes in the monoclinic space group $P2_1$. The unit cell comprises two clusters and twelve DMF molecules. The distances between central Fe^{3+} ion and three peripheral Fe^{3+} ions are also slightly different. The Fe···Fe distances are 3.218(2) Å for Fe1–Fe2, 3.226(2) Å for Fe1–Fe3, and 3.214(2) Å for Fe1–Fe4. Three edges of the iron triangle are not exactly the same, with 5.603(2) Å for Fe2–Fe3, 5.584(2) Å for Fe3–Fe4, and 5.537(2) Å for Fe4–Fe2. The coordination environment of the central Fe1 ion has *pseudo* C_3 symmetry with Fe1···O distances ranging from 2.008(5) Å to 2.046(5) Å, and forms a slightly distorted triangular prism. The selected bond distances and angles data for **4*R*** is listed in Table S4.

Compound **5*R*** crystallizes in the monoclinic space group $P2_1$. The unit cell comprises two clusters, twelve DMA molecules. The distances between the central Fe^{3+} ion and three peripheral Fe^{3+} ions are also slightly different. The Fe···Fe distances are 3.232(1) Å for Fe1–Fe2, 3.232(1) Å for Fe1–Fe3, and 3.210(1) Å for Fe1–Fe4. Three edges of the iron triangle are not exactly the same, with 5.372(1) Å for Fe2–Fe3, 5.692(1) Å for Fe3–Fe4, and 5.672(1) Å for Fe4–Fe2. The coordination environment of the central Fe1 ion has pseudo C_3 symmetry with Fe1···O distances ranging from 1.997(3) Å to 2.057(3) Å, and forms a slightly distorted triangular prism. The selected bond distances and angles for **5*R*** are listed in Table S5.

Though the four Fe ions are in same valence, the coordination environment between the central Fe^{3+} ion and the peripheral Fe^{3+} ion are different significantly. Firstly, the central Fe^{3+} ion is 6O coordinated and the peripheral Fe^{3+} ion is 4O2N coordinated. Secondly, the central Fe^{3+} ion is located in slightly distorted triangular prism coordination environment and the peripheral Fe^{3+} ion is located in slightly distorted octahedral coordination environment. The difference of coordination environment between two types of Fe^{3+} ions will be discussed in detail in the magneto-structural correlation study section. In the crystalline state, the Fe^{3+} atoms between neighboring clusters are well separated from each other by Schiff base ligands and solvent molecules.

Dalton Transactions Dynamic Article Links ▶

Cite this: DOI: 10.1039/c0xx00000x

www.rsc.org/xxxxxx

PAPER

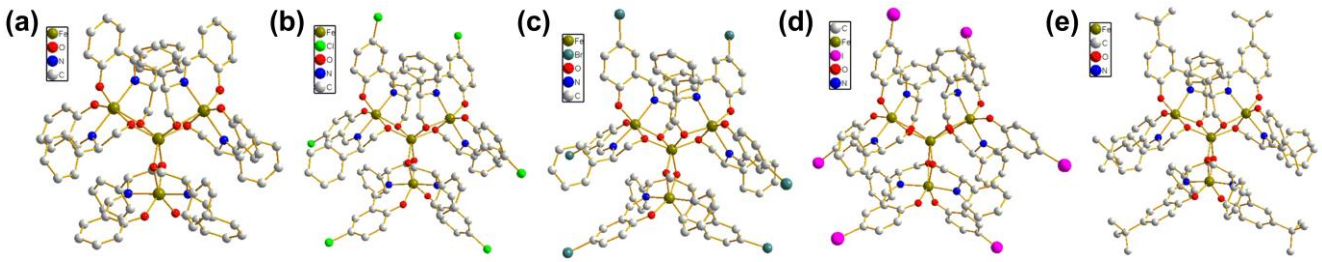

Fig. 1 Crystal structures of compounds **1**–**5** (all *R* configuration). Solvent molecules and hydrogen atoms were omitted for clarity.

Static Magnetic Properties

The temperature dependence of magnetic susceptibility under 1000 Oe dc field was measured for all the six compounds in this paper. For the *R* and *S* enantiomers exhibit identical magnetic responses to dc and ac magnetic field, all the magnetic discussions were concerned only *R* enantiomers in the following. The temperature dependences of the magnetic susceptibility for six compounds all show characteristic of antiferromagnetic clusters with incomplete spin cancellation. For compound **4** as an example, the $\chi_M T$ *vs*. *T* plot is shown in Figure 2. The $\chi_M T$ value is 12.40 cm^3 K mol^{-1} at 300 K and decreases on lowering the temperature, going through a minimum of 11.26 cm^3 K mol^{-1} at $T \approx 170$ K, and then increases to the value of 15.24 cm^3 K mol^{-1} at 16 K. Below this temperature, a sharp decrease is observed. Dc magnetic data for compound **1** has already been presented in ref 13. The $\chi_M T$ *vs*. *T* data of compounds **2**, **3**, and **5** can be seen in the supporting information (see Figure S10-S12). These results all indicate the occurrence of an antiferromagnetic coupling between the central high spin Fe^{3+} ion and the three peripheral high spin Fe^{3+} ions, which leads to a ground state with $S = 5$. It means that three peripheral spins aligned parallel to each other but antiparallel to the central one (see Figure 3). For compound **4** as an example, the observed $\chi_M T$ value at the maximum (15.25 cm^3 K mol^{-1}) is in good agreement with the value of 15.00 cm^3 K mol^{-1} expected for $S = 5$ with $g = 2.0$.

The framework of four Fe^{3+} ions in all five compounds is in the same star shaped topology. Actually, in each compound, the distances between the central Fe^{3+} ion and the peripheral Fe^{3+} ions have slight differences. Magnetic measurements show that these small differences have minor effect to the magnetic coupling interactions of this series Fe^{III}_4 clusters. For clarity, we assume there are two kinds of magnetic interactions within the core of this series compounds, named J_1 and J_2, representing the exchange coupling between the central Fe^{3+} ion and the peripheral Fe^{3+} ion, and between the adjacent peripheral Fe^{3+} ions, respectively. The HDVV spin Hamiltonian can be expressed as follows:

$$\boldsymbol{H} = -2J_1(\boldsymbol{S}_1\cdot\boldsymbol{S}_2 + \boldsymbol{S}_1\cdot\boldsymbol{S}_3 + \boldsymbol{S}_1\cdot\boldsymbol{S}_4) - 2J_2(\boldsymbol{S}_1\cdot\boldsymbol{S}_2 + \boldsymbol{S}_1\cdot\boldsymbol{S}_2 + \boldsymbol{S}_1\cdot\boldsymbol{S}_2) + g\mu_B\boldsymbol{S}\cdot H \quad (1)$$

The $\chi_M T$ *vs*. *T* magnetic data for the five Fe^{III}_4 compounds were fitted by a least-squares fitting procedure with Levenberg–Marquardt algorithm using the program MAGPACK.[23] The best fitted parameters in the temperature range 10–300 K of all compounds are listed in Table 2. The values of J_1 are in the range of –11.4 cm^{-1} for **2** to –13.2 cm^{-1} for **5**, which indicate the antiferromagnetic interactions of central and peripheral Fe^{3+} ions. Small values of J_2 from 0.25 cm^{-1} for **5** to 0.41 cm^{-1} for **4** suggest weak ferromagnetic coupling interactions between adjacent peripheral Fe^{3+} ions. These results demonstrate that the magnetic interactions within the five Fe^{III}_4 compounds are in the same type and within the similar strength.

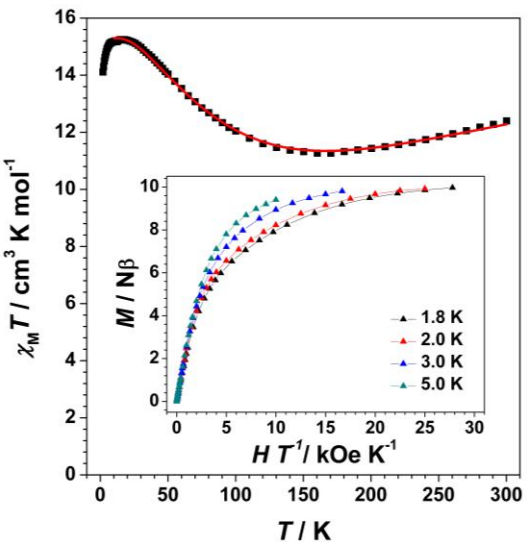

Fig. 2 Temperature dependence of $\chi_M T$ at $H = 1$ kOe at 2–300 K. (The red solid line represents the best simulation of magnetic susceptibilities by MAGPACK at 10–300 K.) Inset is the *M* *vs*. *H*/*T* plots at different temperature (1.8 K, 2.0 K, 3.0 K, and 5.0 K) for the polycrystalline sample of **5**.

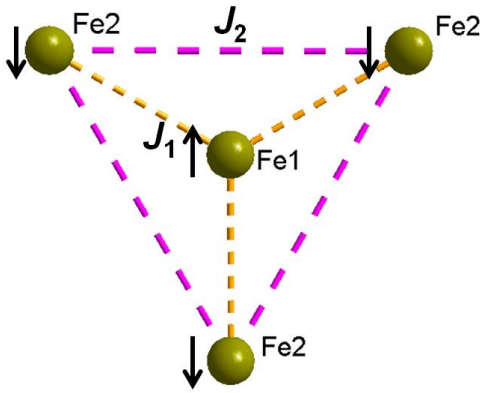

Fig. 3 The star shaped topology of four Fe^{3+} ions, the arrows show the spin configuration in the ground $S = 5$ state of the molecule, J_1 represents the exchange coupling between the central Fe^{3+} ion and the peripheral Fe^{3+} ion, J_2 represents the exchange coupling between the peripheral Fe^{3+} ions.

Isothermal magnetization data were collected in field up to 50 kOe at different low temperature (1.8, 2.0, 3.0, and 5.0 K). The *M vs. H/T* curves of these compounds all display significant bifurcation, which indicates the presence of an appreciable magnetic anisotropy in the ground state (see inset of Figure 2). Considering the spin ground state anisotropy by using the phenomenological spin Hamiltonian $\boldsymbol{H} = D\boldsymbol{S}_z^2 + E(\boldsymbol{S}_x^2 - \boldsymbol{S}_y^2) + g_{iso}\mu_B\boldsymbol{S}\cdot\boldsymbol{B}$, the magnetic data was fit using the program ANISOFIT 2.0.[24] The produced axial and transverse zero-field splitting parameters *D* and *E* are listed in Table 3, which show the sequence of zero-field splitting parameter *D* value is **4** (I) > **1** (H) > **3** (Br) > **2** (Cl) ≈ **5** (*t*-Bu). Small transverse zero-field splitting contributions exist in all five compounds, which is the origin of zero-field quantum tunneling of magnetization.

Table 2 Summary of magnetic coupling data of compound **1**–**5** fitted by MAGPACK

	1 (H)	**2** (Cl)	**3** (Br)	**4** (I)	**5** (*t*-Bu)
J_1	–11.7	–11.4	–12.4	–11.6	–13.2
J_2	0.29	0.34	0.32	0.41	0.25
g	1.99	2.02	2.01	2.02	2.02

Magnetization hysteresis is one of the most important static magnetic characteristic of the magnetic bistability of SMMs. The hysteresis measurements of five compounds were performed at low temperature (0.5–0.6 K) with the help of a ^{3}He system. Figure 4 illustrates butterfly-shaped hysteresis loops emerge in compound **1**, **3**, and **4**. The coincidences of hysteresis loop around $H = 0$ point is mainly due to the presence of fast quantum tunneling of magnetization (QTM). The QTM mechanism promotes magnetization reversal of spin carrier when the magnetic field near zero. Surprisingly, although the structure and magnetic coupling properties are similar to other three compounds, the hysteresis loop was not observed for compounds **2** and **5** at the same temperature range. These results confirm SMM behavior of this series of Fe^{III}_4 clusters at very low temperature.

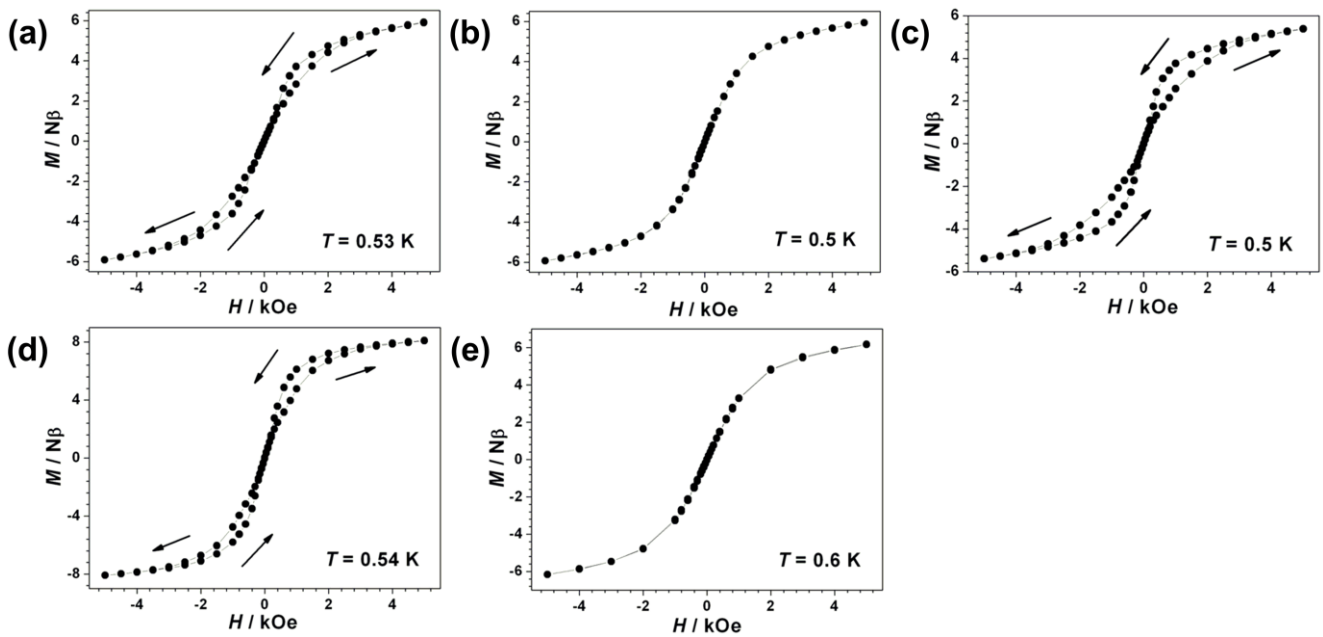

Fig. 4 Plot of magnetization (*M*) vs dc magnetic field (*H*) within ±5 kOe for compound **1**–**6** at 0.5–0.6 K.

Dynamic Magnetic properties

Frequency dependence of χ_{ac}'' is another important characteristic of the magnetic bistability of SMMs in addition to the hysteresis loop. For all five compounds, the alternating-current (ac) susceptibility at various frequencies (from 1 to 1000 Hz) in the absence of a dc field has been investigated (see Figure 5). Both in-phase (χ') and out-of-phase (χ'') susceptibilities of compound **1**-**5** show frequency dependence at low temperature, which indicate they all show SMMs behavior. However, no peak of χ'' appears for **2** and only one peak appears in the χ'' curve of ν = 1000 Hz for **5**, so the relaxation barrier of these two compounds cannot be obtained in the current stage. For the other three compounds, the maximal temperature of frequency peak is found to be highest for **4** and decrease in the order of **4** (I) > **3** (Br) >**1** (H). This result implies that **4** possess the highest anisotropy

barrier. The peak temperature of χ'' of three compounds can be fitted by Arrhenius law (see Figure 6), the parameters U_{eff} and τ_0 evaluated by a linear fit are listed in Table 3. As expected, the fitting results of **4** (I) give $\tau_0 = 2.5 \times 10^{-8}$ and $U_{eff} = 11.0$ K, which possess the highest relaxation barrier in this series compounds. The barrier is a little smaller than that calculated value ($|D|S^2$ = 13.0 K, S is the ground state spin; D is the axial zero-field splitting parameter fitted from M *vs*. H/T plots). The anisotropy barrier is in the order of **4** (I) > **3** (Br) > **1** (H). The τ_0 value indicates the superparamagnetic behavior of this series compounds.

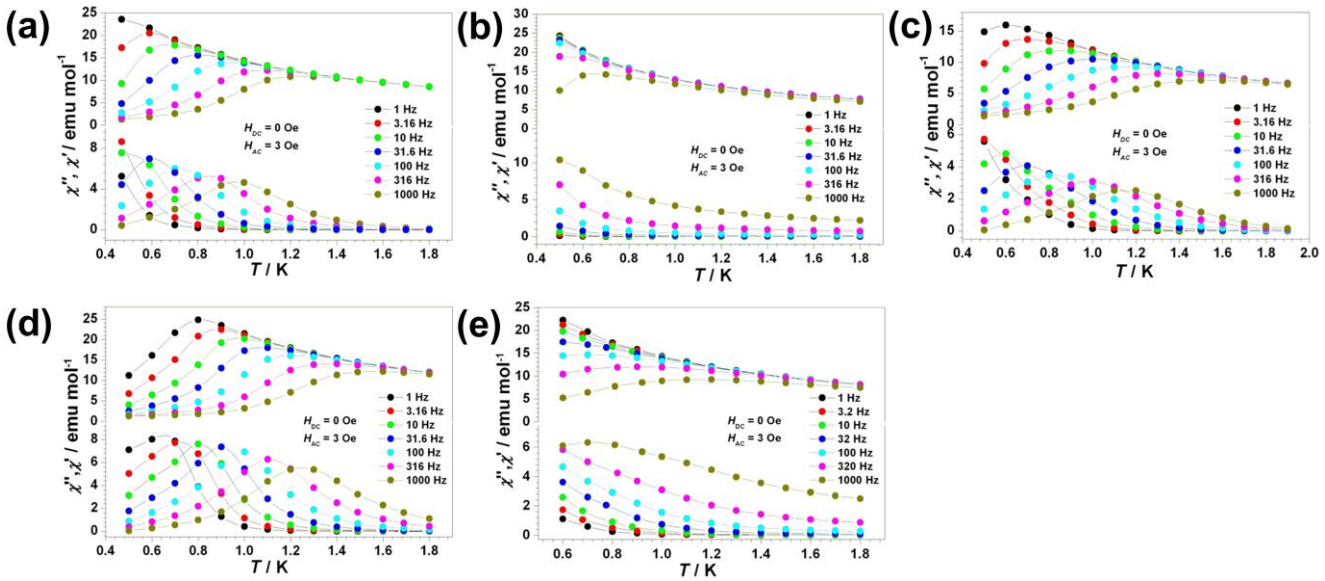

Fig. 5 Temperature dependence of ac susceptibility at frequencies from 1 to 1000 Hz for **1** to **5**.

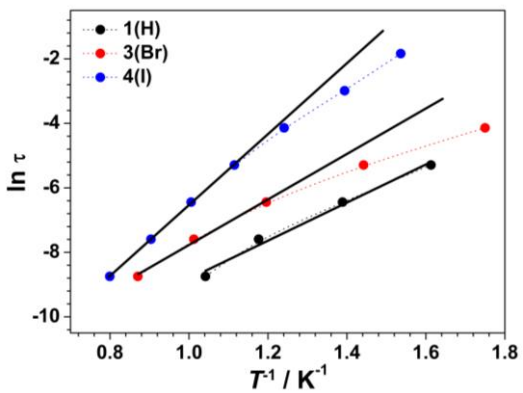

Fig. 6 Arrhenius plots for compounds **1** (H), **3** (Br), and **4** (I) obtained from ac susceptibility measurements in the absence of a dc field.

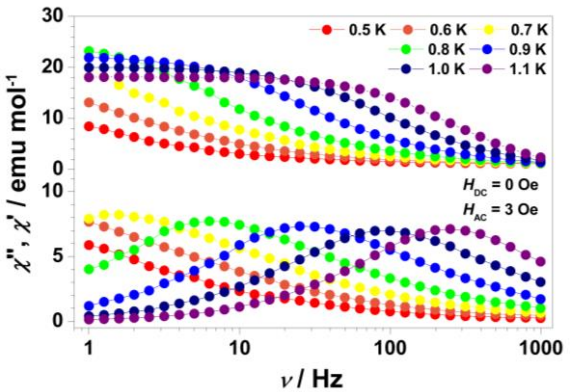

Fig. 7 Frequency dependence of ac susceptibility at frequencies from 1 to 1000 Hz for **4**.

The frequency dependence of the ac susceptibility for compound **4** with high anisotropy barrier was also investigated in the absence of an applied field at the low temperature range. Similar to the temperature dependence data, the curves of χ' and χ'' signals all display significant frequency dependence, and one peak in each curve indicates only one thermal relaxation process exist (see Figure 7). The relaxation energy barrier fitted by Arrhenius law is 10.6 K for **4** (see Figure S13). It is consistent with the values from χ'' *vs*. T measurements.

To inspect the distribution of the relaxation time, the χ'' *vs*. χ' data of **4** at different temperatures (0.5-1.1 K) in the absence of a dc field were fitted by the modified Debye Model (see Figure 8). The resulting α values varies in the range of 0.15-0.29 (the α value indicates deviation from the pure Debye model), which is within the range of superparamagnetism (see Table S6). It suggests the presence of an almost uniformly distributed relaxation process in the range of the measured temperature.

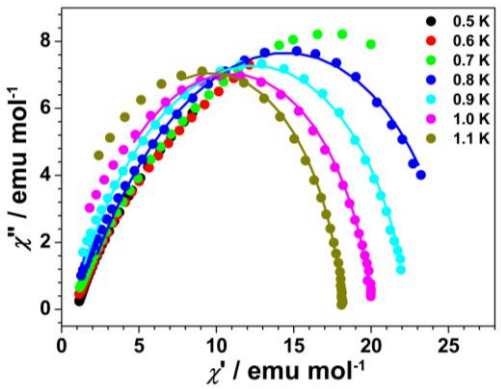

Fig. 8 Cole-Cole plot of **4** in the absence of a dc field at low temperature; the solid lines are the best fit obtained with a modified Debye model.

Table 3 Summary of axial and transverse zero-field splitting parameter *D*, *E*, U_{eff} and τ_0 of compound **1**–**5**

Complex	**1** (H)	**2** (Cl)	**3** (Br)	**4** (I)	**5** (*t*-Bu)
D^a (cm^{-1})	–0.34	–0.29	–0.33	–0.36	–0.29
E^a (cm^{-1})	1.0×10^{-4}	5.2×10^{-5}	5.2×10^{-5}	9.1×10^{-5}	7.8×10^{-5}
g^a	2.01	2.06	2.04	2.07	2.04
D^b (cm^{-1})	–0.34	–0.28	–0.27	–0.29	–0.26
E/D^b	0.0429	0.0244	0.0397	0.0426	0.0148
U_{eff} (K)	5.9	/	7.0	11.0	/
τ_0	4.0×10^{-7}	/	3.7×10^{-7}	2.5×10^{-8}	/

[a] *D* and *E* values fitted by ANISOFIT with giant spin model;

[b] *D* and *E* values calculated by DFT method at B3LYP/TZVP level of theory.

Magneto–structural Correlation Studies

Magnetic studies demonstrated that the anisotropy barrier can be successfully tuned by introducing different substituent in the ligand. In this series of Fe^{III}_4 clusters, the energy barrier of **3** and **4** are higher than that of archetype compound **1**. Compound **4** possesses the highest relaxation barrier (U_{eff} = 11.0 K), which is comparable to the Fe^{III}_4 family compounds with high relaxation barrier reported by Gatteschi, Sessoli, and Cornia et al.[6] Their researches demonstrated that the relaxation barrier can be enhanced by the replacement of axis tridentate ligand. Our results indicated that modification of remote substituent of ligand can also work. So a question emerges naturally, how does the remote substituent influence the anisotropy energy barrier in this family of Fe^{III}_4 molecules?

The origin of magnetic anisotropy is the first question need be answered. As the detailed structure discussions in the section of solid-state structure, the central Fe^{3+} ion and peripheral Fe^{3+} ions are in the very different coordination environment (see Figure 9). The central Fe^{3+} ion are located in slightly distorted triangular prism coordination environment. For example, the central Fe^{3+} ion in these series complexes have *pseudo* C_3 symmetries. Previous study revealed that the high order axial symmetry at least C_3 or D_3 symmetry can minimize the quantum tunneling of magnetization and enhance anisotropy barrier significantly.[6,25] The three peripheral Fe^{3+} ions, however, are very different, which are located in slightly distorted octahedral coordination environment. This type of coordination mode of peripheral Fe^{3+} ion can also produce magnetic anisotropy by the distortion of coordination sphere, which may produce minor contribution to the *D* value of the whole molecule. For convenience of the following theoretical study, we proposed a preliminary model that assumed the contribution of magnetic anisotropy in this series of molecules mainly comes from the central Fe^{3+} ion.

Theoretical calculation was carried out to study the magnetic anisotropy of central Fe^{3+} ion. DFT calculations at B3LYP/TZVP level were used to obtain the axial zero-field splitting parameter *D* and *D*/*E* (*E*: transverse zero-field splitting parameter) of the central Fe^{3+} ions. The calculated *D* values are well consistent with the fitting results by ANISOFIT which considers the whole molecule (see Table 3). This result supports our assumption that the magnetic anisotropy mainly comes from the central Fe^{3+} ion Also, the differences between fitting and DFT results demonstrate the contribution of three peripheral Fe^{3+} ions cannot be neglected.

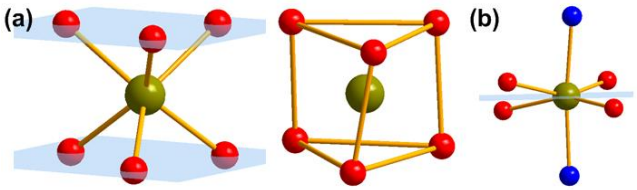

Fig. 9 The coordination environment of (a) central Fe^{3+} ion and (b) peripheral Fe^{3+} ion.

Since the main contribution of magnetic anisotropy comes from the central Fe^{3+} ion, the difference of the central Fe^{3+} ion's coordination environment may be the crucial factor to affect the magnetic anisotropy. In these Fe^{III}_4 molecules, the central Fe^{3+} ions are in the slightly distorted-triangular-prism coordination environment. According to Neumann's Principle,[26] the C_3 axis of the molecule must be one of the magnetic principal axes. Since this molecule behaves a typical SMM behavior, it is reasonable to claim that this C_3 axis is the unique easy axis. The derivation to ideal symmetry can cause the transverse zero-field splitting contribution, which may reduce the effective anisotropy energy barrier through the quantum tunneling of magnetization (QTM). The degree of derivation from triple prism can be analyzed by a quantitative method named "Continuous Symmetry Measures", developed by Alvarez and Avnir et al. It is an effective mathematical method to describe the derivation to the standard symmetry of coordination sphere.[27] By using this method, we obtained the deviation parameter *P* (defined by equation 2) of central Fe^{3+} ion and three peripheral Fe^{3+} ions in compound **1**-**5** according to the derivation from trigonal prism and octahedron, respectively. The results demonstrate that the coordination symmetry of central Fe^{3+} ion approaches trigonal prism and that of peripheral Fe^{3+} ion approaches octahedron. For the central Fe^{3+} ion, the value of derivation parameter to trigonal prism is found to be lowest for **1** and increases in the order **1** < **2** < **3** ≈ **4** < **5**. The central Fe^{3+} ion in **1** possesses the higher symmetry in this series compounds.

$$P(\mathrm{sym}) = 100\frac{\sum_{i=0}^{n-1}\| P_i^{'} - \hat{P}^{'} \|^2}{n} \qquad (2)$$

The intermolecular interaction between the neighboring clusters is another factor to reduce the anisotropy barrier. The intermolecular interaction may cause antiferromagnetic coupling between the paramagnetic carriers in the neighboring cluster at

low temperature. Through the carefully observation of packing mode of compound **1**, **2**, and **3**, the π–π stacking of the benzene ring between the neighboring cluster was found (see Figure S14-S16), which can transmit weak antiferromagnetic coupling and decrease the relaxation barrier. However, duo to the steric effect of functional group I and *t*-Bu, no apparent intermolecular interaction can be formed in compound **4** and **5**. Though the central Fe^{3+} ions in compound **1**–**3** also have the relatively high symmetries, the possible higher magnetic anisotropy barrier may be reduced by the intermolecular interaction. So it may be an effective approach to obtain the Fe^{III}_4 SMMs with a high anisotropy barrier by increasing the axial symmetry and eliminating the intermolecular interaction simultaneously.

Table 4 The continuous symmetry measures results of compound **1**–**5**.

No	**1** (H)	**2** (Cl)	**3** (Br)	**4** (I)	**5** (*t*-Bu)
Fe_1[a]	0.550	0.811	0.979	0.986	1.077
Fe_1[b]	16.059	13.671	12.597	12.509	12.328
Fe_2[a]	9.166	8.483	8.033	6.984	7.863
Fe_2[b]	2.800	3.375	3.448	3.897	3.657
Fe_3[a]	9.172	8.443	7.138	8.442	7.074
Fe_3[b]	3.114	3.131	3.707	3.253	4.258
Fe_4[a]	9.559	8.843	8.428	8.046	8.365
Fe_4[b]	2.608	3.128	3.293	3.405	2.943

[a] Trigonal prism; [b] Octahedron

Circular Dichroism (CD) Spectrum Studies

The optical activity and enantiomeric nature of compounds **2*R***/**2*S*** was confirmed by circular dichroism (CD) spectra, in both solution and solid-state. In DMF solution, the spectrum of **2*R*** exhibits a positive Cotton effect at λ_{max} = 281, 345, and 396 nm and the negative signal at λ_{max} = 315, 440, and 520 nm, while **2*S*** shows Cotton effects of the opposite sign at the same wavelengths (see Figure 10). The peak shape and position of **2*R***/**2*S*** is very similar to that of **1*R***/**1*S*** in ref 13. The CD signals of the pair compounds form a clear mirror image, which also indicates that they are enantiomeric compounds. The solid-state CD spectra gave similar signals as those in solution, which revealed that the optical activity in solution and solid-state is consistent (see Figure S17).

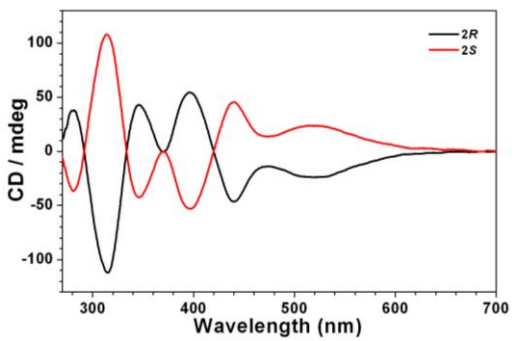

Fig. 10 CD spectra of **2*R*** and **2*S*** at 298 K (5 × 10^{-5} M, DMF).

Conclusions

In summary, a new family of enantiopure star-shape Fe^{III}_4 clusters with different chiral Schiff-base ligand derivatives has been synthesized and magnetically characterized. All five compounds show SMMs behavior. Systematic magnetic studies revealed that the SMM properties can be tuned by the little change of ligand. The iodine derivate compound **4** possesses the highest relaxation barrier. Magneto-structural correlation analysis demonstrated that the coordination symmetry of central Fe^{3+} ion and the intermolecular interaction are two key factors to affect the SMM properties. Compounds with higher axial symmetry and less intermolecular exchange interaction between neighboring molecules may possess the larger magnetic relaxation barrier, which is helpful to design and predict new SMMs in this series. To deeply understanding the magnetic anisotropy in detail in this series Fe^{III}_4 clusters, the comprehensive DFT calculation which consider the contribution of peripheral Fe^{3+} ions, the HF-EPR study and single crystal magnetic characterization are underway, and will be reported in the near future. Also, the magnetic studies of single-molecule and single-molecule layer that applied in spintronics are in progress.

Acknowledgement

This work was supported by the NSFC (21071008, 21321001, 21371043, and 21302035), BJSFC (2122023), and the National Basic Research Program of China (2010CB934601, 2013CB933401). Y.-Y. Zhu is thankful for the financial support by the Open Fund of Beijing National Laboratory for Molecular Sciences (BNLMS). We thank Dr. X. Hao, Ms. L. Wang and Ms. T.-L. Liang (ICCAS) for the X-ray measurement and Dr J.-H. Jia and Dr N. Li for help in structure refinement.

Notes and references

[a]*Key Laboratory of Advanced Functional Materials and Devices, Anhui Province, and School of Chemical Engineering, Hefei University of Technology, Hefei, 230009, P. R. China.*

[b]*Beijing National Laboratory for Molecular Sciences, State Key Laboratory of Rare Earth Materials Chemistry and Applications, College of Chemistry and Molecular Engineering, Peking University, Beijing 100871, P. R. China. Fax: (+86)10-6275-1708; Tel: (+86)10-6276-7569; E-mail: gaosong@pku.edu.cn, bwwang@pku.edu.cn.*

† Electronic Supplementary Information (ESI) available: Experimental procedures, structure and magnetic characterization, Fig. S1-17, Table S1-S6, and the cif file for **1**-**5**. For ESI and crystallographic data See DOI: 10.1039/b000000x/

1 (a) R. Sessoli, H. L. Tsai, A. R. Schake, S. Wang, J. B. Vincent, K. Folting, D. Gatteschi, G. Christou and D. N. Hendrickson, *J. Am. Chem. Soc*., 1993, **115**, 1804. (b) R. Sessoli, D. Gatteschi, A. Canesch and M. A. Novak, *Nature*, 1993, **365**, 141. (c) D. Gatteschi, A. Caneschi, L. Pardi and R. Sessoli, *Science*, 1994, **265**, 1054. (d) S. M. J. Aubin, S. Spagna, H. J. Eppley, R. E. Sager, K. Folting, G. Christou and D. N. Hendrickson, *Mol. Cryst. Liq. Cryst. A*, 1997, **305**, 181. (e) H. J. Eppley, S. M. J. Aubin, M. W. Wemple, D. M. Adams, H. L. Tsai, V. A. Grillo, S. L. Castro, Z. M. Sun, K. Floting, J. C. Huffman, D. N. Hendrickson and G. Christou, *Mol. Cryst. Liq. Cryst. A*, 1997, **305**, 167. (f) D. Gatteschi, R. Sessoli and J. Villain, *Molecular Nanomagnets*; Oxford University Press: Oxford, 2006.

2 (a) T. C. Stamatatos, K. A. Abboud, W. Wernsdorfer and G. Christou, *Angew. Chem. Int. Ed*., 2008, **47**, 6694. (b) E. C. Yang, W. Wernsdorfer, L. N. Zakharov, Y. Karaki, A. Yamaguchi, R. M. Isidro, G. D. Lu, S. A. Wilson, A. L. Rheingold, H. Ishimoto and D. N. Hendrickson, *Inorg. Chem*., 2006, **45**, 529. (c) H. Oshio, M. Nihei, S. Koizumi, T. Shiga, H. Nojiri, M. Nakano, N. Shirakawa and M. Akatsu, *J. Am. Chem. Soc*., 2005, **127**, 4568. (d) L. Lecren, O. Roubeau, C. Coulon, Y. G. Li, X. F. Le Goff, W. Wernsdorfer, H. Miyasaka and R. Clérac, *J. Am. Chem. Soc*., 2005, **127**, 17353. (e) M. H. Zeng, M. X. Yao, H. Liang, W. X. Zhang and X. M. Chen, *Angew. Chem. Int. Ed*., 2007, **46**, 1832. (f) Y. Z. Zhang, W. Wernsdorfer, F.

Pan, Z. M. Wang and S. Gao, *Chem. Commun.*, 2006, 3302. (g) C. J. Milios, R. Inglis, A. Vinslava, R. Bagai, W. Wernsdorfer, S. Parsons, S. P. Perlepes, G. Christou and E. K. Brechin, *J. Am. Chem. Soc.*, 2007, **129**, 12505. (h) C. J. Milios, A. Vinslava, W. Wernsdorfer, S. Moggach, S. Parsons, S. P. Perlepes, G. Christou and E. K. Brechin, *J. Am. Chem. Soc*., 2007, **129**, 2754. (i) A. M. Ako, I. J. Hewitt, V. Mereacre, R. Clérac, W. Wernsdorfer, C. E. Anson, and A. K. Powell, *Angew. Chem. Int. Ed*., 2006, **45**, 4926.

3 (a) W. Wernsdeorfer and R. Sessoli, *Science*, 1999, **284**, 133. (b) M. N. Leuenberger and D. Loss, *Nature*, 2001, **410**, 789. (c) L. Bogani and W. Wernsdorfer, *Nat. Mater*., 2008, **7**, 179. (d) W. Wernsdorfer, *C. R. Chimie*., 2008, **11**, 1086. (e) J. J. Henderson, C. Koo, P. L. Feng, E. del Barco, S. Hill, I. S. Tupitsyn, P. C. E. Stamp and D. N. Hendrickson, *Phy. Rev. Lett*., 2009, **103**, 017202.

4 (a) P. Artus, C. Boskovic, J. Yoo, W. E. Streib, L. C. Brunel, D. N. Hendrickson and G. Christou, *Inorg. Chem.*, 2001, **40**, 4199. (b) C. Boskovic, M. Pink, J. C. Huffman, D. N. Hendrickson and G. Christou, *J. Am. Chem. Soc*., 2001, **123**, 9914. (c) M. Soler, P. Artus, K. Folting, J. C. Huffman, D. N. Hendrickson and G. Christou, *Inorg. Chem*., 2001, **40**, 4902. (d) M. Pacchioni, A. Cornia, A. C. Fabretti, L. Zobbi, D. Bonacchi, A. Caneschi, G. Chastanet, D. Gatteschi and R. Sessoli, *Chem. Commun*., 2004, 2604. (e) T. Kuroda-Sowa, S. Fukuda, S. Miyoshi, M. Maekawa, M. Munakata, H. Miyasaka and M. Yamashita, *Chem. Lett*., 2002, 682. (f) G. Q. Bian, T. Kuroda-Sowa, H. Konaka, M. Hatano, M. Maekawa, M. Munakata, H. Miyasaka and M. Yamashita, *Inorg. Chem*., 2004, **40**, 4790.

5 For Mn_6 series SMMs paper, see: (a) C. J. Milios, C. P. Raptopoulou, A. Terzis, F. Lloret, R. Vicente, S. P. Perlepes and A. Escuer, *Angew. Chem. Int. Ed*., 2004, **43**, 210. (b) C. J. Milios, A. Vinslava, A. G. Whittaker, S. Parsons, W. Wernsdorfer, G. Christou, S. P. Perlepes and E. K. Brechin, *Inorg. Chem*., 2006, **45**, 5272. (c) C. J. Milios, M. Manoli, G. Rajaraman, A. Mishra, L. E. Budd, F. White, S. Parsons, W. Wernsdofer, G. Christou and E. K. Brechin, *Inorg. Chem*., 2006, **45**, 6782. (d) C. J. Milios, A. Vinslava, P. A. Wood, S. Parsons, W. Wernsdorfer, G. Christou, S. P. Perlepes and E. K. Brechin, *J. Am. Chem. Soc*., 2007, **129**, 8. (e) C. J. Milios, A. Vinslava, W. Wernsdorfer, S. Moggach, S. Parsons, S. P. Perlepes, G. Christou and E. K. Brechin, *J. Am. Chem. Soc*., 2007, **129**, 2754. (f) C. J. Milios, R. Inglis, A. Vinslava, R. Bagai, W. Wernsdorfer, S. Parsons, S. P. Perlepes, G. Christou and E. K. Brechin, *J. Am. Chem. Soc*., 2007, **129**, 12505. (g) A. R. Tomsa, J. M. Lillo, Y. L. Li, L. M. Chamoreau, K. Boubekeur, F. Farias, M. A. Novak, E. Cremades, E. Ruiz, A. Proust, M. Verdaguer and P. Gouzerh, *Chem. Commun*., 2010, **46**, 5106. (h) C.-L. Zhou, Z.-M. Wang, B.-W. Wang and S. Gao, *Polyhedron*, 2011, **30**, 3279.

6 For Fe^{III}_4 series SMMs paper, see: (a) A. L. Barra, A. Caneschi, A. Cornia, F. Fabrizi de Biani, D. Gatteschi, C. Sangregorio, R. Sessoli and L. Sorace, *J. Am. Chem. Soc*., 1999, **121**, 5302. (b) R. W. Saalfrank, I. Bernt, M. M. Chowdhry, F. Hampel and G. B. M. Vaughan, *Chem.–Eur. J*., 2001, **7**, 2765. (c) A. Cornia, A. C. Fabretti, P. Garrisi, C. Mortalò, D. Bonacchi, D. Gatteschi, R. Sessoli, L. Sorace, W. Wernsdorfer and A. L. Barra, *Angew. Chem. Int. Ed*., 2004, **43**, 1136. (d) M. Moragues-Cánovas, E. Rivière, L. Ricard, C. Paulsen, W. Wernsdorfer, G. Rajaraman, E. K. Brechin and T. Mallah, *Adv. Mater*., 2004, **16**, 1101. (e) N. T. Madhu, J.-K. Tang, I. J. Hewitt, R. Clérac, W. Wernsdorfer, J. van Slageren, C. E. Anson and A. K. Powell, Polyhedron, 2005, **24**, 2864. (f) S. Accorsi, A. L. Barra, A. Caneschi, G. Chastanet, A. Cornia, A. C. Fabretti, D. Gatteschi, C. Mortalò, E. Olivieri, F. Parenti, P. Rosa, R. Sessoli, L. Sorace, W. Wernsdorfer and L. Zobbi, *J. Am. Chem. Soc*., 2006, **128**, 4742. (g) A.-L. Barra, F. Bianchi, A. Caneschi, A. Cornia, D. Gatteschi, L. Gorini, L. Gregoli, M. Maffini, F. Parenti, R. Sessoli, L. Sorace and A. M. Talarico, *Eur. J. Inorg. Chem.*, 2007, 4145. (h) A. Cornia, L. Gregoli, C. Danieli, A. Caneschi, R. Sessoli, L. Sorace, A. L. Barra and W. Wernsdorfer, *Inorg. Chim. Acta*., 2008, **361**, 3481. (i) L. Gregoli, C. Danieli, A. L. Barra, P. Neugebauer, G. Pellegrino, G. Poneti, R. Sessoli and A. Cornia, *Chem.–Eur. J*., 2009, **15**, 6456. (j) R. Singh, A. Banerjee, E. Colacio and K. K. Rajak, *Inorg. Chem.*, 2009, **48**, 4753. (h) M.J. Rodriguez-Douton, A. Cornia, R. Sessoli, L. Sorace and A.-L. Barra, *Dalton Trans*., 2010, **39**, 5851.

7 H. U. Güdel and U. Hauser, *Inorg. Chem*., 1980, **19**, 1325.

8 (a) N. Reddig, M. U. Triller, D. Pursche, A. Rompel and B. Krebs, *Z. Anorg. Allg. Chem*., 2002, **628**, 2458. (b) E.-Q. Gao, S.-Q. Bai, H. Zheng and C.-H. Yan, *Inorg. Chem*., 2005, **44**, 677. (c) S. Khanra, K. Kuepper, T. M. Weyhermüller, M. Prinz, M. Raekers, S. Voget, A. V. Postnikov, F. M. F. de Groot, S. J. George, M. Coldea, M. Coldea, M. Neumann and P. Chaudhuri, *Inorg. Chem*., 2008, **47**, 4605.

9 V. Pavlishchuk, F. Birkelbach, T. Weyhermüller, K. Wieghardt and P. Chaudhuri, *Inorg. Chem*., 2002, **41**, 4405.

10 M. Prinz, K. Kuepper, C. Taubitz, M. Raekers, S. Khanra, B. Biswas, T. Weyhermüller, M. Uhlarz, J. Wosnitza, J. Schnack, A. V. Postnikov, C. Schröder, S. J. George, O. M. Neumann and P. Chaudhuri, *Inorg. Chem*., 2010, **49**, 2093.

11 (a) E. Tancini, M. J. Rodriguez-Douton, L. Sorace, A.-L. Barra, R. Sessoli and A. Cornia, *Chem.–Eur. J*., 2010, **16**, 10482. (b) P. Totaro, K. C. M. Westrup, M.-E. Boulon, G. G. Nunes, D. F. Back, A. Barison, S. Ciattini, M. Mannini, L. Sorace, J. F. Soares, A. Cornia and R. Sessoli, *Dalton Trans*., 2013, **42**, 4416.

12 Y.-Y. Zhu, C. Cui, Y.-Q. Zhang, J.-H. Jia, X. Guo, C. Gao, K. Qian, S.-D. Jiang, B.-W. Wang, Z.-M. Wang and S. Gao, *Chem. Sci*., 2013, **4**, 1802.

13 Y.-Y. Zhu, X. Guo, C. Cui, B.-W. Wang, Z.-M. Wang and S. Gao, *Chem. Commun*., 2011, **47**, 8049.

14 (a) G. G. Condorelli, A. Motta, G. Pellegrino, A. Cornia, L. Gorini, I. L. Fragala, C. Sangregorio and L. Sorace, *Chem. Mater*., 2008, **20**, 2405; (b) G. Pellegrino, A. Motta, A. Cornia, I. Spitaleri, I. L. Fragala and G. G. Condorelli, *Polyhedron*, 2009, **28**, 1758.

15 (a) M. Mannini, F. Pineider, Ph. Sainctavit, C. Danieli, E. Otero, C. Sciancalepore, A. M. Talarico, M. A. Arrio, A. Cornia, D. Gatteschi and R. Sessoli, *Nat. Mater*., 2009, **8**, 194. (b) F. Pineider, M. Mannini, C. Danieli, L. Armelao, F. M. Piras, A. Magnani, A. Cornia and R. Sessoli, *J. Mater. Chem*., 2010, **20**, 187. (c) M. Mannini, F. Pineider, C. Danieli, F. Totti, L. Sorace, Ph. Sainctavit, M. A . Arrio, E. Otero, L. Joly, J. C. Cezar, A. Cornia and R. Sessoli, *Nature*, 2010, **468**, 417. (d) M. J. Rodriguez-Douton, M. Mannini, L. Armelao, A.-L. Barra, E. Tancini, R. Sessoli and A. Cornia, *Chem. Commun*., 2011, **47**, 1467.

16 L. Bogani, C. Danieli, E. Biavardi, N. Bendiab, A. L. Barra, E. Dalcanale, W. Wernsdorfer and A. Cornia, *Angew. Chem. Int. Ed*., 2009, **48**, 746.

17 H. Amouri and M. Gruselle, *Chirality in Transition Metal Chemistry*: *Molecules*, *Supramolecular Assemblies and Materials*, John Wiley & Sons Ltd, 2008, 215–224.

18 For examples of chiral molecule-based magnets, see: (a) M. Minguet, D. Luneau, E. Lhotel, V. Villar, C. Paulsen, D. B. Amabilino and J. Veciana, *Angew. Chem. Int. Ed*., 2002, **41**, 586. (b) K. Inoue, K. Kikuchi, M. Ohba and H. Õkawa, *Angew. Chem. Int. Ed*., 2003, **42**, 4810. (c) E. Coronado, C. J. Gómez-García, A. Nuez, F. M. Romero and J. C. Waerenborgh, *Chem. Mater*., 2006, **18**, 2670. (d) A. Beghidja, P. Rabu, G. Rogez and R. Welter, *Chem.–Eur. J*., 2006, **12**, 7627. (e) H.-R. Wen, C.-F. Wang, Y.-Z. Li, J.-L. Zuo, Y. Song and X.-Z. You, *Inorg. Chem*., 2006, **45**, 7032. (f) M.-H. Zeng, B. Wang, X.-Y. Wang, W.-X. Wang, X.-M. Chen and S. Gao, *Inorg. Chem*., 2006, **45**, 7069. (g) W. Kaneko, S. Kitagawa and M. Ohba, *J. Am. Chem. Soc*., 2007, **129**, 248. (h) C. M. Zaleski, E. C. Depperman, J. W. Kampf, M. L. Kirk and V. L. Pecoraro, *Inorg. Chem*., 2006, **45**, 10022. (i) C.-M. Liu, R.-G. Xiong, D.-Q. Zhang and D.-B. Zhu, *J. Am. Chem. Soc*., 2010, **132**, 4044. (j) E. Pardo, C. Train, R. Lescouezec, Y. Journaux, J. Pasan, C. Ruiz-Perez, F. S. Delgado, R. Ruiz-Garcia, F. Lloretd and C. Paulsene, *Chem. Commun*., 2010, **46**, 2322.

19 (a) G. L. J. A. Rikken and E. Raupach, *Nature*, 1997, **390**, 493. (b) G. L. J. A. Rikken and E. Raupach, *Nature*, 2000, **405**, 932. (c) C. Train, R. Gheorghe, V. Krstic, L. M. Chamoreau, N. S. Ovanesyan, G. L. J. A. Rikken, M. Gruselle and M. Verdaguer, *Nat. Mater*., 2008, **7**, 729. (c) Y. Kitagawa, H. Segawa and K. Ishii, *Angew. Chem. Int. Ed*. 2011, **39**, 9133.

20 (a) E.-Q. Gao, S.-Q. Bai, Z.-M. Wang and C.-H. Yan, *J. Am. Chem. Soc*., 2003, **125**, 4984. (b) E.-Q. Gao, Y.-F. Yue, S.-Q. Bai, Z. He and C.-H. Yan, *J. Am. Chem. Soc*., 2004, **126**, 1419. (c) X.-L. Tong, T.-L. Hu, J.-P. Zhao, Y.-K. Wang, H. Zhang and X.-H. Bu, *Chem. Commun*., 2010, **46**, 8543. (d) R. Inglis, F. White, S. Piligkos, W.

Wernsdorfer, E. K. Brechin and G. S. Papaefstathiou, *Chem. Commun*., 2011, **47**, 3090. (e) B. Liu, H. B. Zheng, Z. M. Wang and S. Gao, *CrystEngComm*., 2011, **13**, 5285.

21 G. M. Sheldrick, SHELXS-97; University of Gottingen: Gottingen, Germany, 1990.

22 G. M. Sheldrick, SHELXS-97; University of Gottingen: Gottingen, Germany, 1997.

23 J. J. Borrás-Almenar, J. M. Clemente-Juan, E. Coronado and B. S. Tsukerblat, *Inorg. Chem*., 1999, **38**, 6081.

24 M. P. Shores, J. J. Sokol, J. R. Long, *J. Am. Chem. Soc*., 2002, **124**, 2279.

25 Y.-Z. Zheng, W. Xue, W.-X. Zhang, M.-L. Tong and X.-M. Chen, *Inorg. Chem*., 2007, **46**, 6437.

26 M. Gerloch, *Magnetism and Ligand-field Analysis*, Cambridge University Press, 1984.

27 (a) H. Zabrodsky, S. Peleg and D. Avnir, *J. Am. Chem. Soc*., 1992, **114**, 7843. (b) M. Pinsky and D. Avnir, *Inorg. Chem*., 1998, **37**, 5575. (c) D. Casanova, J. Cirera, M. Liunell, P. Alemany, D. Avnir, S. Alvarez, *J. Am. Chem. Soc*., 2004, **126**, 1755. (d) S. Alvarez, D. Avnir, M. Llunell, M. Pinsky, *New J. Chem*., 2002, **26**, 996. (e) S. Alvarez, P. Alemany, D. Casanova, J. Cirera, M. Llunell, D. Avnir, *Coord. Chem. Rev*., 2005, **249**, 1693.

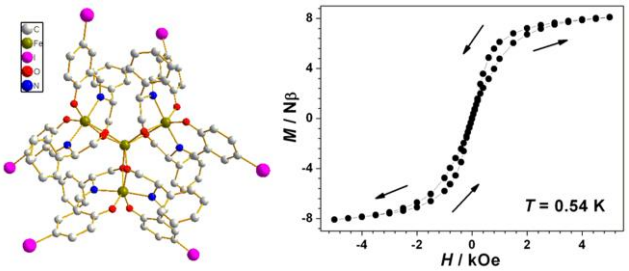

We report a new family of enantiopure star-shaped Fe^{III}_4 single-molecule magnets (SMMs). Interestingly, the SMM properties of this series clusters can be finely tuned by the remote substituent of the ligands.